Modeling of the Skywalker X8 Fixed-Wing UAV: Flight Tests and System Identification

Dirk Reinhardt, Kristoffer Gryte, Tor Arne Johansen
Department of Engineering Cybernetics, *Norwegian University of Science and Technology*, Trondheim, Norway
{dirk.p.reinhardt, kristoffer.gryte, tor.arne.johansen}@ntnu.no

***Abstract*—This paper proposes a combination of wind-tunnel tests and flight experiments to find an aerodynamic model of the Skywalker X8 airframe. The static coefficients resulting from wind-tunnel tests are augmented with a parsimonious damping model that we find by using flight test data and a sequentially thresholded least squares algorithm. Experimental results show significant improvements to the pre-existing baseline model.**

***Index Terms*—System Identification, Unmanned Aircraft, Aerodynamic Model**

I. Introduction

A. Motivation and Background

In this paper, we address some issues that became apparent when using the model of the Skywalker X8 proposed by Gryte et al. [1], as it seems that our experiments were the first to use this model in a model-based controller and evaluate in flight tests. In [1], Gryte et al. auto-validate the identified models against the measured wind tunnel data, resulting in favorable scores of the coefficient of determination very close to 1. However, the resulting score is even negative when we compared the accelerations obtained through the force model and the observations based on flight data from inertial measurement units (IMUs). This indicates that using the original model [1] in a model-based controller may not optimize performance. Considering that the targeted use-case by Gryte et al. is model-based flight control or model-based estimation of aerodynamic parameters, we see it crucial to apply the fitness metric to relevant flight data.

With a closer look at the wind tunnel data that serves as a foundation for the following model identification process, we identified several possible modifications that can improve the model. First, the lever arm of the attack point of the force vector to the center of mass is implicit in the model. Gryte et al. tweaked the vector describing the lever arm to have the pitch moment aligned with their experience. We instead explicitly model the generalized forces at the aerodynamic reference point, the location of the force sensors during the experiments, and identify the vector to center of mass based on flight data. Second, we have a more thorough look at the subset of the available data suitable for identifying aerodynamic linear coefficients related to the side-slip angle. Moreover, we reduce the drag model's complexity and simultaneously improve its fitness. Third, the final set of parameters proposed by Gryte et al. is a blend of parameters identified by the wind tunnel, results from a Vortex-Lattice method (XFLR), and additional manual tweaks to the parameters based on experience from flight experiments. The result is a set of parameters that is not optimal in either of the original identification procedures. We present a different approach that combines the use of wind tunnel and flight data, which leads to a coherent parameter

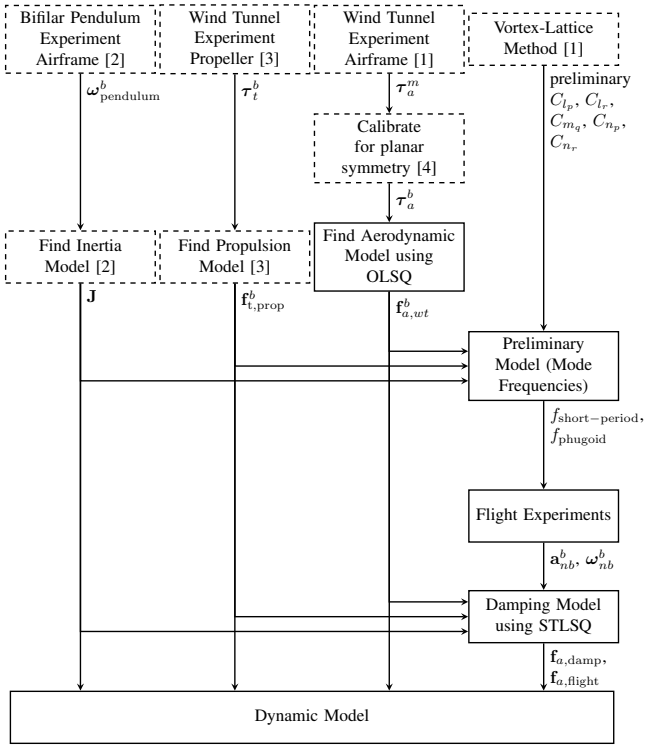

Fig. 1. Overview of the modeling work. Steps that are in solid rectangles are contributions in this article and dashed rectangles represent results that have been published in the references. Given that the model structure of the aerodynamic coefficients that can be obtained from wind tunnel experiments is well-understood, we use ordinary least squares (OLSQ) in this identification step. To allow for more flexibility with respect to the model structure, we use a second order polynomial library and a sequentially thresholded least squares algorithm (STLSQ) to find the damping model based on flight data.

This work has been carried out at the Center for Autonomous Marine Operations and Systems (NTNU-AMOS) and was supported by the Research Council of Norway through the Centers of Excellence funding scheme, grant no. 223254 - NTNU AMOS, and no. 261791 AutoFly. Corresponding author: Dirk Reinhardt

Fig. 2. Skywalker X8.

vector, see Figure 1.

This paper aims to find an improved model by dealing with the outlined shortcomings of the described identification process. A significant part of the model will be re-identified based on the same wind tunnel data used by Gryte et al. [1]. However, instead of finding the damping coefficients for the rotational motion through a Vortex-Lattice method, we use actual flight data. Finally, evaluate the new model compared to the baseline model from Gryte et al. [1] and a model entirely based on the estimated coefficients from the flights.

B. Related Work

This paper is not the first to consider the aerodynamic model of the X8. In addition to [1], which is a continuation of [5], several publications consider this popular airframe. Farhadi et al. [6] identify a lateral model of the X8 using flight data, in a combination of the output-error method and ordinary least squares regression. Gan et al. [7] identify the static aerodynamic coefficients from a Reynolds-averaged Navier-Stokes (RANS) computational fluid dynamics (CFD) program. Winter et al. [8] also provide a RANS CFD analysis, further using time-series CFD simulations to study the effect on the dynamic coefficients in situations where the airfoil is subject to ice aggregation. All three papers rely to some extent on our previous work [1], [5]. System identification based on flight data is also a well-established field [9], [10], and has been widely used in modelling of fixed-wing unmanned aerial vehicles (UAVs), both in the time- [11], [12] and frequency domain [13], [14]. More recently, Kaiser et al. [15] presented results where they identify the longitudinal dynamics of a fighter aircraft using the Sparse Identification of Nonlinear Dynamics (SINDy) proposed by Brunton et al. [16].

C. Contribution

We improve the aerodynamic model proposed in [1], hereafter referred to as baseline model, by re-using the available wind tunnel data. We transform the data to increase its planar symmetry and use flight data to find the dynamic coefficients instead of the previously applied Vortex-Lattice method. The improved model is made available to the research community on github[1].

[1]https://github.com/krisgry/x8

II. Method

A. The Dataset

The experiments conducted by Gryte et al. are thoroughly described in [1]. The collected dataset includes variations of the airspeed, angle of attack, and sideslip angle, as well as control surface deflections. The tests were based on the assumption of decoupled dynamics in the lateral and longitudinal plane at small aerodynamic angles. This means that it includes rotations of the lateral plane at zero angle of attack, and rotations of the longitudinal plane at zero sideslip angle. The angle of attack was varied between $-10\,\mathrm{deg}$ and $15\,\mathrm{deg}$ with some measurements at higher values and low airspeeds to identify forces in the stall regime. Gryte et al. [1] tested five uniformly distributed elevator deflections between $-20\,\mathrm{deg}$ and $20\,\mathrm{deg}$ at airspeeds set to either $18\,\mathrm{m/s}$ or $21\,\mathrm{m/s}$. With zero aileron deflection and sideslip angle, the data points available for the identification of the longitudinal coefficients are given by

$$(V_a,\, \alpha,\, \delta_e) \in \{18, 21\} \times [-10, 15] \times \{-20, -10, 0, 10, 20\}, \tag{1}$$

where V_a, α, and δ_e denote airspeed, angle of attack and elevator deflections, respectively. The dataset for identifying the lateral coefficients includes sideslip angle variations within $-15\,\mathrm{deg}$ and $15\,\mathrm{deg}$ at the same airspeeds as for the longitudinal tests. Based on the assumption of the aileron to be symmetric around zero, the dataset only includes negative deflections. At zero elevator deflection and angle of attack, the lateral data points are given by

$$(V_a,\, \beta,\, \delta_a) \in \{18, 21\} \times [-15, 15] \times \{-20, -10, 0\}, \tag{2}$$

where β and δ_a denote sideslip angle and aileron deflection, respectively. Forces and moments due to the vehicle's weight were compensated during each run. The airframe was carefully mounted onto the force sensor to align the measurement axes with the axes of the body-fixed frame. The remaining mis-alignment between the measurement frame and the body-fixed frame was accounted for through a calibration routine which we describe in a separate paper.

B. Dataset for Model Identification

The aerodynamic force coefficients were computed based on the measured body-fixed forces, airspeed and geometric factors. The body-fixed forces $X,\, Y,\, Z \in \mathbb{R}$ are transformed to the forces referred to as drag, crosswind and lift, denoted by $D,\, C,\, L \in \mathbb{R}$ as follows:

$$\mathbf{f}_a^w = \begin{bmatrix} D \\ C \\ L \end{bmatrix} = \mathbf{R}_{bw}(\alpha, \beta)^\top \begin{bmatrix} -X \\ Y \\ -Z \end{bmatrix}. \tag{3}$$

The rotation matrix $\mathbf{R}_{bw} \in \mathrm{SO}(3)$ describes the axes of the wind frame in the coordinates of the body-fixed frame. It is defined as a function of angle of attack and sideslip angle

$$\mathbf{R}_{bw}(\alpha,\, \beta) = \begin{bmatrix} \mathrm{c}(\beta)\mathrm{c}(\alpha) & -\mathrm{s}(\beta)\mathrm{c}(\alpha) & -\mathrm{s}(\alpha) \\ \mathrm{s}(\beta) & \mathrm{c}(\beta) & 0 \\ \mathrm{c}(\beta)\mathrm{s}(\alpha) & -\mathrm{s}(\beta)\mathrm{s}(\alpha) & \mathrm{c}(\alpha) \end{bmatrix}, \tag{4}$$

where we use the shorthand notation $\mathrm{s}(\cdot), \mathrm{c}(\cdot)$ for $\sin(\cdot)$, $\cos(\cdot)$, respectively.

The moments about the roll, pitch and yaw axes are denoted by l, m, $n \in \mathbb{R}$ and given in the body-fixed frame. The dimensionless coefficients are given by

$$C_D = \frac{D}{\bar{q} S_{\text{wing}}}, \quad C_C = \frac{C}{\bar{q} S_{\text{wing}}}, \quad C_L = \frac{L}{\bar{q} S_{\text{wing}}}$$
$$C_l = \frac{l}{\bar{q} S_{\text{wing}} b}, \quad C_m = \frac{m}{\bar{q} S_{\text{wing}} c}, \quad C_n = \frac{n}{\bar{q} S_{\text{wing}} b}, \tag{5}$$

where $S_{\text{wing}}, b, c \in \mathbb{R}$ denote the wing surface, wing span and mean chord length, respectively. The coefficients are plotted in Figure 3 for their respective variations of the control surfaces and aerodynamic angles. Higher angles of attack measurements beyond those used for model identification are included in the figures to determine the linear region below the stall angle. We see that for identifying a linear model in C_L and C_m, the angle of attack measurements need to be restricted to angles below $12\,\text{deg}$, which is referred to as stall angle.

Having a look at the lateral coefficients, we can see that nonlinear effects are notable for sideslip angles that are either below $-5\,\text{deg}$ or above $5\,\text{deg}$. The nonlinearities appear negligible for roll and pitch moment, but are clearly visible for the yaw moment. Regarding zero aileron deflections, identifying the yaw moment coefficient would in the case of ideal measurements lead to a model that is invariant to sideslip angle variations. Moreover, the effect of aileron deflections on the yaw moment coefficient seems to be saturated for aileron deflections below $-10\,\text{deg}$ (or above $10\,\text{deg}$ due to symmetry), which should be considered when selecting a subset of the data for identification of a model for C_n that is linear in δ_a. None of these effects are taken into account by Gryte et al. [1].

1) Model structure: We modify the structure of the existing model with alterations to the drag coefficient. For now, we focus on a subset of the aerodynamic coefficients that can be identified based on wind tunnel experiments in which the airframe is statically mounted to a pan-tilt-unit. The dynamic coefficients that capture effects of the angular rate are therefore not included. The expressions for the identifiable aerodynamic coefficients are given by

$$\begin{aligned}
C_D &= C_{D_0} + C_{D_\alpha}\alpha + C_{D_{\alpha\delta_e}}\alpha\delta_e + C_{D_{\alpha^2}}\alpha^2 \\
C_C &= C_{C_0} + C_{C_\beta}\beta + C_{C_{\delta_a}}\delta_a \\
C_L &= C_{L_0} + C_{L_\alpha}\alpha + C_{L_{\delta_e}}\delta_e \\
C_l &= C_{l_0} + C_{l_\beta}\beta + C_{l_{\delta_a}}\delta_a \\
C_m &= C_{m_0} + C_{m_\alpha}\alpha + C_{m_{\delta_e}}\delta_e \\
C_n &= C_{n_0} + C_{n_\beta}\beta + C_{n_{\delta_a}}\delta_a.
\end{aligned} \tag{6}$$

The model of the drag coefficient does not include the effects of sideslip, given that the sensitivity of the drag force to sideslip angle variations was not significant. We also replace the quadratic elevator term by a mixed term with the angle of attack, reflecting the fact that a negative/positive elevator deflection at a positive angle of attack actually decreases/increases the area of the UAV that is orthogonal to the air stream.

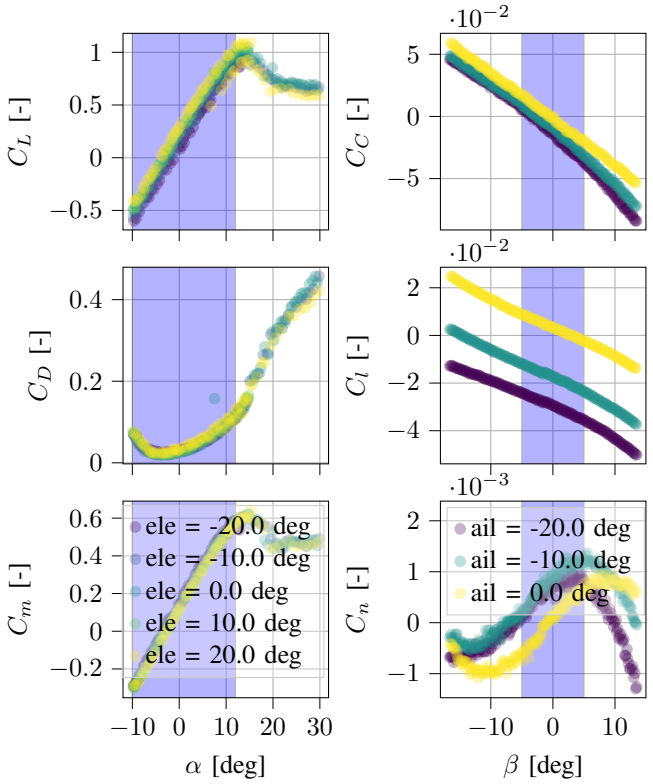

Fig. 3. Measured aerodynamic coefficients for varying aerodynamic angles and surface deflections. The moment coefficients in the right column are with respect to the sensor position. The interval of the angle of attack $[-10\,\text{deg}, 12\,\text{deg}]$ and the sideslip angle $[-5\,\text{deg}, 5\,\text{deg}]$ (marked in blue) are suitable for identification of a linear model.

TABLE I
PARAMETERS OF THE WIND TUNNEL MODEL

C_{D_0}	0.023617	C_{m_0}	0.051656	C_{L_0}	0.058192
C_{D_α}	0.012051	C_{m_α}	2.409198	C_{L_α}	3.996278
$C_{D_{\alpha\delta_e}}$	0.075081	$C_{m_{\delta_e}}$	-0.043286	$C_{L_{\delta_e}}$	0.242942
$C_{D_{\alpha 2}}$	1.725632				
C_{l_0}	0.001839	C_{C_0}	-0.002544	C_{n_0}	0.000058
C_{l_β}	-0.064541	C_{C_β}	-0.23371	C_{n_β}	0.006828
$C_{l_{\delta_a}}$	0.094302	$C_{C_{\delta_a}}$	0.036065	$C_{n_{\delta_a}}$	-0.004462

Remark 1. Gryte et al. [1] also saw a notable drop in the coefficient of determination for the drag model when auto-validating it against the wind tunnel measurements. They however assumed misalignment of the airframe to be the issue and did not conclude that the aerodynamic coefficient is not significantly affected by sideslip angle variations.

2) Identification of the model parameters: The model structure in (6) is well-suited for linear regression which can

be used to identify models of the form

$$\mathbf{z} = \mathbf{X}\boldsymbol{\Theta} + \boldsymbol{\epsilon} \tag{7}$$

where $\mathbf{z} \in \mathbb{R}^N$ is a vector of N measurements, $\mathbf{X} \in \mathbb{R}^{N \times p}$ is the regressor matrix composed of the model terms, and $\boldsymbol{\Theta} \in \mathbb{R}^p$ is the vector of model parameters. The part of the measurements that are not explained by the model are captured by the residual $\boldsymbol{\epsilon} \in \mathbb{R}^N$. Gauss showed that a cost function composed of the sum of squares of the residuals

$$J(\boldsymbol{\Theta}) = \frac{1}{2}(\mathbf{z} - \mathbf{X}\boldsymbol{\Theta})^\top (\mathbf{z} - \mathbf{X}\boldsymbol{\Theta}), \tag{8}$$

is minimized by the solution

$$\hat{\boldsymbol{\Theta}} = (\mathbf{X}^\top \mathbf{X})^{-1} \mathbf{X}^\top \mathbf{z}. \tag{9}$$

To find an estimate of the parameter vector $\hat{\boldsymbol{\Theta}}$ for the drag coefficient model, we use the regressor matrix and measurement vector

$$\mathbf{X}_D = \begin{bmatrix} 1 & \alpha_i & \alpha_i \delta_{e_i} & \alpha_i^2 \\ \vdots & \vdots & \vdots & \vdots \\ 1 & \alpha_N & \alpha_N \delta_{e_N} & \alpha_N^2 \end{bmatrix}, \quad \mathbf{z} = \begin{bmatrix} C_{D_i} \\ \vdots \\ C_{D_N} \end{bmatrix}. \tag{10}$$

The parameters of the other coefficients are identified in the same way by parameterizing the regressor matrix and measurement vector according to the model structure in (6). A problem with ordinary least squares is that it will fit the given parameter vector to the measurements, regardless of how well its elements explain them, which requires a good confidence in the proposed model structure. Regarding the preceding discussion of the measurements, it is clear that a linear model is appropriate for all coefficients except the drag coefficient, which also requires quadratic terms. The resulting model parameters are summarized in Table I and plotted against the measurements in Figure 4. The linear models correlate well with the measured data in general. The notable exception is the yaw moment coefficient where a model that is linear in the aileron deflection significantly differs from the measurements at higher deflections. The drag coefficient model could be extended by polynomial terms of the angle of attack up to order four to better capture the data at negative angles. Negative angles of attack are usually not part of the nominal flight conditions, and we prioritize model simplicity over global accuracy in this case.

The coefficients C_l, C_m, C_n model the aerodynamic moments at the point where the sensor was located during the wind tunnel experiments. Let this point be referred to as the *aerodynamic reference point*. This is in contrast to [1], that propose a model with respect to the center of mass of the airframe. The position of the point of the force measurements relative to the center of mass was manually adjusted until the equilibrium point of the pitch moment was shifted to an angle of attack that approximately matched the experience from flight tests. Instead of implicitly assuming a fixed offset, we identify the vector based on data collected in flight tests. The identification of this lever arm, together with a suitable

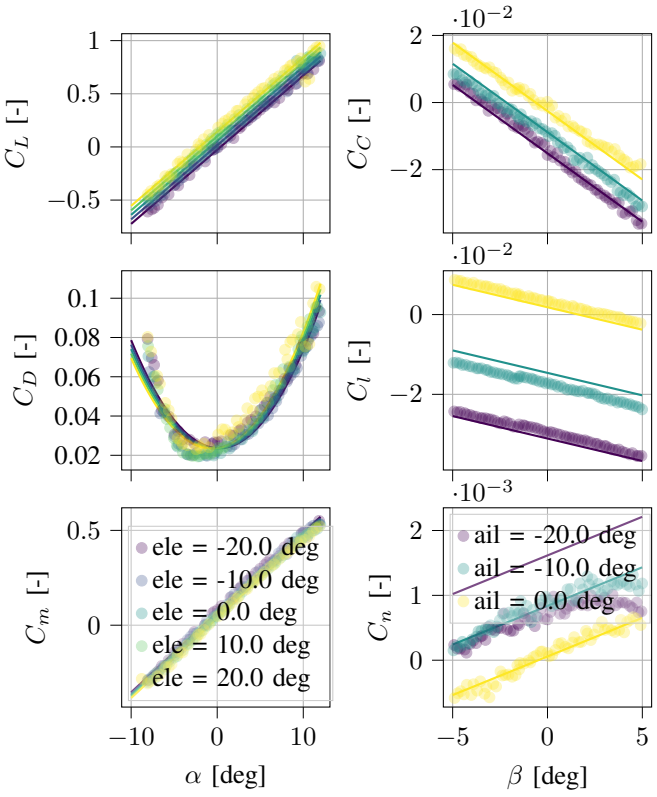

Fig. 4. Aerodynamic models based on the wind tunnel data compared to the measurements for sweeps of angle of attack and sideslip angle. The moment coefficients are with respect to the sensor position.

model that augments the wind tunnel model with additional damping, is the subject of the next section.

III. Model Augmentation Based on Flight Experiments

So far, we have found an aerodynamic model based on data from a wind tunnel. The wind tunnel model maps relative linear velocities and the surface deflections to aerodynamic forces and moment, and is denoted by $\mathbf{f}_{\text{wt}} : \mathbb{R}^5 \mapsto \mathbb{R}^6$ which reads as

$$\begin{bmatrix} \mathbf{f}^w_{a,\text{wt}} \\ \mathbf{m}^b_{a,\text{wt}} \end{bmatrix} = \mathbf{f}_{\text{wt}}(\boldsymbol{\nu}^b_r, \delta_a, \delta_e) \tag{11}$$

The aim of this section is to use data collected during flight experiments to augment $\mathbf{f}_{\text{wt}}$ with a damping model that further considers the effect of angular velocities onto the generalized aerodynamic forces. We thus seek a function $\mathbf{f}_{\text{damp}} : \mathbb{R}^6 \mapsto \mathbb{R}^6$, and the final augmented model $\mathbf{f}_{\text{wt,aug}} : \mathbb{R}^8 \mapsto \mathbb{R}^6$ such that the modeled generalized aerodynamic forces are given by

$$\begin{aligned} \begin{bmatrix} \mathbf{f}^w_{a,\text{wt,aug}} \\ \mathbf{m}^b_{a,\text{wt,aug}} \end{bmatrix} &= \mathbf{f}_{\text{wt,aug}}(\boldsymbol{\nu}^b_r, \delta_a, \delta_e) \\ &= \mathbf{f}_{\text{wt}}(\mathbf{v}^b_r, \delta_a, \delta_e) + \mathbf{f}_{\text{damp}}(\boldsymbol{\nu}^b_r). \end{aligned} \tag{12}$$

We will further identify a separate model that is entirely based on the collected flight data and includes effects of the

throttle δ_t. Let this model be denoted by $\mathbf{f}_{\text{flight}} : \mathbb{R}^9 \mapsto \mathbb{R}^6$ and it's resulting forces be given by

$$\begin{bmatrix} \mathbf{f}^w_{a,\text{flight}} \\ \mathbf{m}^b_{a,\text{flight}} \end{bmatrix} = \mathbf{f}_{\text{flight}}(\boldsymbol{\nu}^b_r, \boldsymbol{\delta}), \quad \text{with } \boldsymbol{\delta} = \begin{bmatrix} \delta_a & \delta_e & \delta_t \end{bmatrix}^\top. \tag{13}$$

A brief outline of the flight experiments to identify the new models reads as follows: Starting from wings-level horizontal flight, we induced oscillations of the control surfaces as a chirp signal with frequency range from $4\,\text{Hz}$ to $8\,\text{Hz}$ and minimum and maximum set to $-5\,\text{deg}$ and $5\,\text{deg}$, respectively. We moreover used step signals that were added as doublets to the elevators and in the form of 1-2-1 signals to the ailerons as depicted in Figure 5. The relative velocities from Ardupilot's wind velocity observer, IMU data and actuator set-points are recorded and used for the following identification procedure.

We assume that a model of the propulsion is available that maps airspeed and throttle set-point to a propulsion force and let the result be denoted by $\mathbf{f}^b_{\text{t,prop}} \in \mathbb{R}^3$. For example the propulsion force model identified in [3] models the propulsion force vector $\mathbf{f}^b_{\text{t,prop}} = \begin{bmatrix} T & 0 & 0 \end{bmatrix}^\top$ with

$$\begin{aligned} C_T &= \delta_t(V_a + \delta_t(k_m - V_a))(k_m - V_a) \\ T &= \rho S_{\text{prop}} \eta_{\text{prop}} C_T. \end{aligned} \tag{14}$$

The propeller parameters are $S_{\text{prop}} = 0.108$, $\eta_{\text{prop}} = 0.248$ and the electric motor parameter is $k_m = 37.42$. For more details on the identified thrust model, see [3]. A last assumption on existing models is knowledge of the moment of inertia $\mathbf{J}^b$, which has been identified based on bifilar pendulum tests and is given by

$$\mathbf{J}^b = \begin{bmatrix} 0.335 & 0 & -0.029 \\ 0 & 0.14 & 0 \\ -0.029 & 0 & 0.40 \end{bmatrix} \tag{15}$$

The observed generalized aerodynamic forces are then computed by combining several measurements as

$$\mathbf{f}^w_{a,z} = m\mathbf{R}_{bw}{}^\top \mathbf{a}^b_{nb} - \mathbf{f}^b_{\text{t,prop}} \tag{16}$$

$$\mathbf{m}^b_{a,z} = \mathbf{J}^b \dot{\boldsymbol{\omega}}^b_{nb} - \mathbf{J}^b \boldsymbol{\omega}^b_{nb} \times \boldsymbol{\omega}^b_{nb}, \tag{17}$$

where $\mathbf{a}^b_{nb} \in \mathbb{R}^3$ denotes the linear acceleration measured by the IMU and m denotes the mass of the UAV. The observed angular acceleration $\dot{\boldsymbol{\omega}}^b_{nb} \in \mathbb{R}^3$ is computed using the centered difference formula based on the observed angular velocity.

In the following section we will first discuss how to find a lever arm between the center of mass and the aerodynamic reference point, i.e. the position of the measurement equipment in the wind tunnel tests. The lever arm will be used to correct the moments of the wind tunnel model. After that follows a discussion on how to find the damping model, $\mathbf{f}_{\text{damp}}$, and the model that is fully identified based on flight data, $\mathbf{f}_{\text{flight}}$.

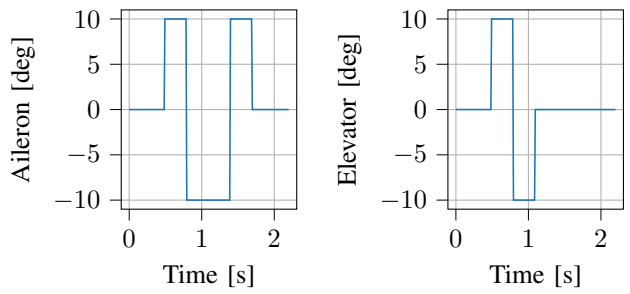

Fig. 5. Step inputs used in the flight experiments for model identification and evaluation.

A. Distance from Aerodynamic Reference Point to the Center of Mass

Let the coefficients that model the aerodynamic moment at the aerodynamic reference point used in the wind tunnel be denoted by $C_{\{l,m,n\},ar}$ and the values at the center of mass be denoted by $C_{\{l,m,n\},cm}$. Their difference is determined by the lever arm $\mathbf{r}_{ar,cm}$ and the aerodynamic force coefficients as

$$\begin{bmatrix} C_l \\ C_m \\ C_n \end{bmatrix}_{cm} = \begin{bmatrix} C_l \\ C_m \\ C_n \end{bmatrix}_{ar} + \text{diag}(b,c,b)^{-1} \left(\mathbf{r}_{ar,cm} \times \begin{bmatrix} C_X \\ C_Y \\ C_Z \end{bmatrix} \right). \tag{18}$$

The expression follows from simple mechanics of a force-inducing moment given by the cross-product of the lever arm and the force vector.

We can again use linear regression to find $\mathbf{r}_{ar,cm}$ and use the skew-symmetric operator $\mathbf{S}$ to express a cross-product of two vectors $\mathbf{x}$, $\mathbf{y} \in \mathbb{R}^3$ as a matrix operation $\mathbf{x} \times \mathbf{y} = \mathbf{S}(\mathbf{x})\mathbf{y}$. It is defined for a vector $\mathbf{x} = \begin{bmatrix} x_1 & x_2 & x_3 \end{bmatrix}^\top$ as

$$\mathbf{S}(\mathbf{x}) = \begin{bmatrix} 0 & -x_3 & x_2 \\ x_3 & 0 & -x_1 \\ -x_2 & x_1 & 0 \end{bmatrix}. \tag{19}$$

Given N measurements, for each sample i let

$$\mathbf{X}_i = -\text{diag}(b,c,b)^{-1} \mathbf{S} \left(\mathbf{R}_{wb}(\alpha,\beta)^\top \begin{bmatrix} -C_D \\ C_C \\ -C_L \end{bmatrix} \right), \tag{20}$$

$$\mathbf{z}_i = \begin{bmatrix} C_l \\ C_m \\ C_n \end{bmatrix}_z - \begin{bmatrix} C_l \\ C_m \\ C_n \end{bmatrix}_{ar} \tag{21}$$

which can be vertically concatenated to give the regressor matrix $\mathbf{X} \in \mathbb{R}^{3N \times 3}$ and measurement vector $\mathbf{z} \in \mathbb{R}^{3N}$. Using the measured data gives the OLSQ

$$\mathbf{r}_{ar,cm} = \begin{bmatrix} -0.226 & -0.02 & 0.144 \end{bmatrix}, \tag{22}$$

which is in line with the vector found in [1].

Remark 2. Considering the dimensions of the Skywalker X8, an offset of $0.144\,\text{m}$ in the z-direction may seem too high. However, keep in mind that this reflects the different

orientations of the sensor frames of the force balance used in the wind tunnel experiments and the frame of the IMU in the flight experiments.

B. Aerodynamic Models from Flight Observations

In this section, we will first give a brief outline of the method that we use to identify the models $\mathbf{f}_{\text{damp}}$ and $\mathbf{f}_{\text{flight}}$ before briefly showing how to apply it.

1) Sparse Identification of Nonlinear Dynamics: Ordinary least squares that we used up until now has the drawback that it gives a solution that fits the proposed parameter vector to the measurements, even if a subset of the parameters actually does not explain the underlying dynamics in a meaningful way. There are several methods that address this problem by introducing an additional penalty on the size of the coefficients. A prominent method is *Ridge Regression* using an additional l_2 regularization. Other methods such as *Lasso* or *Elastic Net* fit sparse models by including l_1 or l_0 regularization sparse models with fewer terms. In this direction, Brunton et al. [16] developed Sparse Identification of Nonlinear Dynamics (SINDy). Since its first publication in 2016, SINDy received a lot of attention and has recently been made available as an open-source toolbox implemented in Python [17]. The idea is to use a library of symbolic functions such as low-order polynomials and optimize over the induced function space to have a linear combination of nonlinear functions describe the dynamical system that best fits the collected measurement data. The underlying assumption is that the dynamics have a sparse representation in the function space that is described by the library. We use SINDy to find an expression for the damping forces of the airframe, and give a brief outline on how it works.

Consider an autonomous dynamic system that is not affected by external disturbances. It's dynamics can be described by

$$\dot{\mathbf{x}} = \mathbf{f}(\mathbf{x}) \tag{23}$$

for which the function $\mathbf{f}$ is to be determined from data of the state $\mathbf{x}(t)$ and its derivative $\dot{\mathbf{x}}(t)$. The data at sampling times $t_1, t_2, \ldots, t_m$ is arranged into matrices $\mathbf{X}, \dot{\mathbf{X}} \in \mathbb{R}^{m \times n_x}$ given as

$$\mathbf{X} = \begin{bmatrix} \mathbf{x}^\top(t_1) \\ \mathbf{x}^\top(t_2) \\ \vdots \\ \mathbf{x}^\top(t_m) \end{bmatrix}, \qquad \dot{\mathbf{X}} = \begin{bmatrix} \dot{\mathbf{x}}^\top(t_1) \\ \dot{\mathbf{x}}^\top(t_2) \\ \vdots \\ \dot{\mathbf{x}}^\top(t_m) \end{bmatrix}. \tag{24}$$

Then a function library $\boldsymbol{\Theta}(\mathbf{X})$ consisting of nonlinear candidate functions based on $\mathbf{X}$ is used, for example

$$\boldsymbol{\Theta}(\mathbf{X}) = \begin{bmatrix} 1 & \mathbf{X} & \mathbf{X}^{P_2} \end{bmatrix} \tag{25}$$

where the matrix $\mathbf{X}^{P_2}$ includes quadratic nonlinearities:

$$\mathbf{X}^{P_2} = \begin{bmatrix} x_1^2(t_1) & x_1(t_1)x_2(t_1) & \ldots & x_{n_x}^2(t_1) \\ x_1^2(t_2) & x_1(t_2)x_2(t_2) & \ldots & x_{n_x}^2(t_2) \\ \vdots & \vdots & \ddots & \vdots \\ x_1^2(t_m) & x_1(t_m)x_2(t_m) & \ldots & x_{n_x}^2(t_m) \end{bmatrix}. \tag{26}$$

The coefficients $\boldsymbol{\Xi} = [\boldsymbol{\xi}_1 \ \boldsymbol{\xi}_2 \ \ldots \ \boldsymbol{\xi}_{n_x}]$ are then used to set up a sparse regression problem to select the nonlinear candidate functions that model the time-derivatives $\dot{\mathbf{X}}$ through a linear combination of the features that are included in the function library

$$\dot{\mathbf{X}} = \boldsymbol{\Theta}(\mathbf{X})\boldsymbol{\Xi}. \tag{27}$$

The minimization problem seeks the coefficients according to the objective

$$\boldsymbol{\xi}_k = \arg\min_{\boldsymbol{\xi}_k} \|\dot{\mathbf{X}}_k - \boldsymbol{\Theta}(\mathbf{X})\boldsymbol{\xi}_k\|_2 + \alpha\|\boldsymbol{\xi}_k\|_1 \tag{28}$$

where the $\|\cdot\|_1$ promotes sparsity in the function space. A trade-off between low model complexity and sufficient accuracy can be made by tuning the parameter α. The result of the sparse symbolic regression, which is implemented in [17], is the coefficient vector $\boldsymbol{\Xi}$ from which we can construct the governing equations as

$$\dot{x}_k = f_k(\mathbf{x}) \approx \boldsymbol{\Theta}(\mathbf{x}^\top)\boldsymbol{\xi}_k \tag{29}$$

with $\boldsymbol{\Theta}(\mathbf{x})$ denoting the vector of symbolic functions that were proposed as candidates.

2) Damping model augmentation to the wind tunnel model: Now, to find expressions for the damping terms to augment the wind tunnel model, we use the error vectors of the generalized aerodynamic forces. Let the values obtained by the wind tunnel model be denoted by $\mathbf{f}_{a,\text{wt}}^w$, $\mathbf{m}_{a,\text{wt}}^b$. The goal is to find a damping model $\mathbf{f}_{\text{damp}}$ that minimizes a residual $\boldsymbol{\epsilon}$ of the difference between the wind tunnel model and the observations $\mathbf{f}_{a,z}^w$, $\mathbf{m}_{a,z}^b$, which can be formulated as

$$\begin{bmatrix} \mathbf{f}_{a,z}^w - \mathbf{f}_{a,\text{wt}}^w \\ \mathbf{m}_{a,z}^b - \mathbf{m}_{a,\text{wt}}^b \end{bmatrix} = \mathbf{f}_{\text{damp}}(\mathbf{x}) + \boldsymbol{\epsilon}, \quad \text{with } \mathbf{x} = \boldsymbol{\nu}_r^b. \tag{30}$$

with $\boldsymbol{\epsilon}$ being the remaining error.

The variables to explain the errors are the relative velocities $\boldsymbol{\nu}_r^b$, which build the polynomial function library in the form of (25). We used six sequences of oscillating input disturbances to the aileron and elevator over a duration of $15\,\text{s}$ as training data. Finding the error models with the sequentially thresholded least squares (STLSQ) algorithm and $\alpha = 0.05$ with the threshold set to 0.1 gives the coefficient matrix $\boldsymbol{\Xi}$ shown in Table II. The coefficient vectors for the rotational damping model have a desirable sparse structure which shows that a simple model is sufficient to explain the difference between the observed moment and the linear model from the wind tunnel. The coefficient vectors for the force error model are less sparse, which indicates that a function library based on second order polynomials of the relative velocities is not sufficient to capture the difference between the wind tunnel model and the observations. For instance angle of attack, sideslip angle, airspeed or their products are not included. The extension of the feature library to rational polynomials, trigonometric functions or fractional exponents is straight forward and may give models that are more accurate and sparse.

TABLE II
THE COEFFICIENT MATRIX Ξ FOR THE DAMPING AUGMENTATION TO THE WIND TUNNEL MODEL. THE COEFFICIENTS THAT ARE 0 ARE STRUCTURAL ZEROS AND NOT ROUNDED.

	dX	dY	dZ	dl	dm	dn
1	-15.01	-2.88	-398.74	3.22	0.29	0
u	0.52	0.21	48.51	-0.21	0	0
v	0	6.89	18.54	0.66	0	0
w	8.73	2.02	-41.30	0	-0.24	0
p	2.70	2.07	-8.62	-0.67	0	0
q	-5.60	-0.26	50.31	0.16	0.50	0
r	-4.89	-26.10	21.09	32.12	-0.12	-0.18
u^2	0	0	-1.43	0	0	0
uv	0	-0.33	-1.06	0	0	0
uw	-0.48	-0.11	3.04	0	0	0
up	-0.16	-0.14	0.50	0	0	0
uq	0.28	0	-3.30	0	0	0
ur	0.23	1.86	-1.16	-2.16	0	0
v^2	0.16	0	-2.03	0	0	0
vw	0	0.16	-0.72	0	0	0
vp	0	0	-0.17	0	0	0
vq	0	-0.15	0.56	0	0	0
vr	0.85	-0.20	-7.35	0	0	0
w^2	-0.41	0	0.30	0	-0.15	0
wp	0	0.44	0	0.44	0	-0.17
wq	0	0	0.44	0	0.24	0
wr	0.13	0	0.84	0.87	0	0
p^2	-0.26	0	-0.57	0	0	0
pq	0.21	-0.95	-0.48	-0.14	0	0
pr	-0.26	-0.23	-4.86	0.36	-0.66	0.39
q^2	0.86	0	-0.70	0	-0.23	0
qr	-0.53	-0.37	-0.46	-2.52	0	0
r^2	2.77	-0.76	-43.44	-0.49	-0.56	0

Remark 3. The training data can also be used to find the aerodynamic damping coefficients that that were used in [1] by means of ordinary least squares. However, this leads to a degrading fitness compared to the raw wind tunnel model where damping is neglected.

3) Full model of the aerodynamic forces: A model that is identified based on the available flight data can be used for comparison. We seek a model $\mathbf{f}_{\text{flight}}$ for the generalized aerodynamic forces as a function of the relative velocities and the control input $\boldsymbol{\delta} = \begin{bmatrix}\delta_a & \delta_e & \delta_t\end{bmatrix}^\top$. This can be formulated as

$$\begin{bmatrix}\mathbf{f}_{a,z}^{w} \\ \mathbf{m}_{a,z}^{b}\end{bmatrix} = \mathbf{f}_{\text{flight}}(\mathbf{x}) + \boldsymbol{\epsilon} \quad \text{with } \mathbf{x} = \begin{bmatrix}\boldsymbol{\nu}_r^b \\ \boldsymbol{\delta}\end{bmatrix}. \tag{31}$$

with $\boldsymbol{\epsilon}$ being the error. We use the same training data and parameterization of the optimizer as for the damping model. The coefficients of $\mathbf{f}_{\text{flight}}$ are given in Table III. Note again the sparsity of the resulting coefficient vectors, indicating a good choice of the function library. A problem that is apparent in this model is that the data for identification includes mostly constant throttle so that there is little information on how it affects the dynamics. The result of this is the high magnitudes of the coefficients related to the terms that include δ_t. A more rigorous test design would be needed to accurately model the effect of the throttle. During this test campaign, however, the primary purpose was to find the rotational damping coefficients to augment the wind tunnel model. A more thorough identification of a model that is entirely based on data collected in flight is part of future work.

IV. FLIGHT RESULTS AND DISCUSSION

The models are compared against the baseline model presented in [1] in test sequences including chirp signals and step perturbations to elevator and aileron. The modeled aerodynamic forces for the respective disturbances to the aileron and elevator are depicted in Figure 6 and Figure 7. A set of different chirp signals was used to identify the damping model and the full aerodynamic model based on flight data, and no step perturbations were used in the identification process.

We use the coefficient of determination (R^2) as a metric to evaluate the model fitness in terms of the generalized aerodynamic forces and the resulting accelerations. The results are summarized in Table IV. They indicate that our model obtained from the wind tunnel without damping already outperforms the baseline model in all forces except for the side force Y. However, the lateral acceleration $\dot{v}$ shows that the aerodynamic force in this direction is not significant compared to the coriolis term. The damping augmentation further improves the wind tunnel model except for the roll moment l and the resulting acceleration $\dot{p}$. This suggests an overfitting of the roll damping to the training data. Another possible explanation is the feedback controller in the loop that will introduce disturbances into the observations of the open-loop damping. A more rigorous test campaign in which the UAV is operated in open-loop for the collection of the training data can mitigate this problem. Upon inspection of the trajectories depicted in Figure 6 and Figure 7, we see that the roll model from the wind tunnel data is already capturing the most important transients of the observed roll moment, which should be sufficient for model-based control. Similar arguments can be made for the yaw moment n, which in contrast to the roll moment, is improved by the damping augmentation. The most improvements to the wind tunnel model are in the pitch moment m, for which we see drastic improvements by adding a small set of additional terms, as can be seen in Table II.

Regarding the modeled forces X, Y, Z, the R^2 scores and the depicted trajectories show that the wind tunnel model without damping augmentation is a better fit than the baseline model. However, both models appear to capture all relevant transients and thus differ from the observations by a slowly time-varying offset. The variance of this offset is further reduced for the trajectories of the accelerations, which are not shown here. Offset-free control and integral action are well-suited to compensate for this type of model mismatch, such that the additional complexity introduced by the damping augmentation is not necessary for model-based control.

TABLE III
THE COEFFICIENT MATRIX Ξ FOR THE GENERALIZED FORCES IDENTIFIED WITH FLIGHT DATA.

	X	Y	Z	l	m	n
1	27.72	-5.94	-200.19	-8.80	3.19	-1.04
u	-0.97	0.41	23.41	0.52	-0.22	0
v	2.49	-1.81	-15.41	0.20	0	0.50
w	11.27	0	-23.38	-0.64	-0.57	0
p	4.96	3.54	-16.26	0	0	0
q	-10.49	0.23	56.32	0.56	0.86	0
r	20.82	-9.70	-77.45	-5.75	-5.21	-0.52
δ_a	0	0	0.10	0	0	0
δ_e	0	0	0	0	-0.10	0
δ_t	-118.23	17.33	14.27	22.95	-3.23	3.29
u^2	0	0	-0.89	0	0	0
uv	-0.11	0	0.87	0	0	0
uw	-0.66	0	0.98	0	0	0
up	-0.36	-0.17	1.18	0	0	0
uq	0.67	0	-4.15	0	0	0
ur	-1.53	0.76	5.85	0.79	0.31	0
$u\delta_a$	0	0	0	0	0	0
$u\delta_e$	0	0	-0.12	0	0	0
$u\delta_t$	2.20	-0.93	7.05	-1.12	0.37	0
v^2	0	0	0	0	0	0
vw	0.18	0	-0.78	0	0	0
vp	0	0	0	0	0	0
vq	0	0	0.47	-0.10	0	0
vr	-0.39	-0.29	-0.69	0	0	0
$v\delta_a$	0	0	0	0	0	0
$v\delta_e$	0	0	0	0	0	0
$v\delta_t$	-1.40	1.24	3.31	-1.23	0	-0.45
w^2	0.47	0	-0.36	0	0	0
wp	0	0.21	0	0.26	0	0
wq	-0.66	0	1.21	0	0.12	0
wr	2.41	0	-6.73	0.72	0	0
$w\delta_a$	0	0	0	0	0	0
$w\delta_e$	0	0	0	0	0	0
$w\delta_t$	2.02	-0.31	-3.06	0.79	0.28	0
p^2	0	0	-1.36	0	0	0
pq	0	-0.39	0	0	0	0
pr	0.16	0	-3.12	-0.41	-0.62	0
$p\delta_a$	0	0	0	0	0	0
$p\delta_e$	0	0.10	0	0	0	0
$p\delta_t$	2.16	0	-6.49	-0.93	0	0
q^2	0.96	0	-2.36	0	-0.23	0
qr	-2.98	-0.49	4.33	-1.84	0	-0.30
$q\delta_a$	0	0	0	0	0	0
$q\delta_e$	0	0	0	0	0	0
$q\delta_t$	-3.78	0	17.89	-0.42	-0.64	0
r^2	2.61	-2.61	5.17	-2.45	0	0.45
$r\delta_a$	0	0	-0.75	0	0	0
$r\delta_e$	-0.18	0	0.37	0.12	0	0
$r\delta_t$	2.41	-5.04	-19.24	-12.51	0	-0.71
δ_a^2	0	0	0	0	0	0
$\delta_a\delta_e$	0	0	0	0	0	0
$\delta_a\delta_t$	0	0.34	0	0.69	0	0
δ_e^2	0	0	0	0	0	0
$\delta_e\delta_t$	0	0.14	-1.19	0	-0.12	0
δ_t^2	80.40	-1.86	-106.05	-4.67	-2.28	-2.86

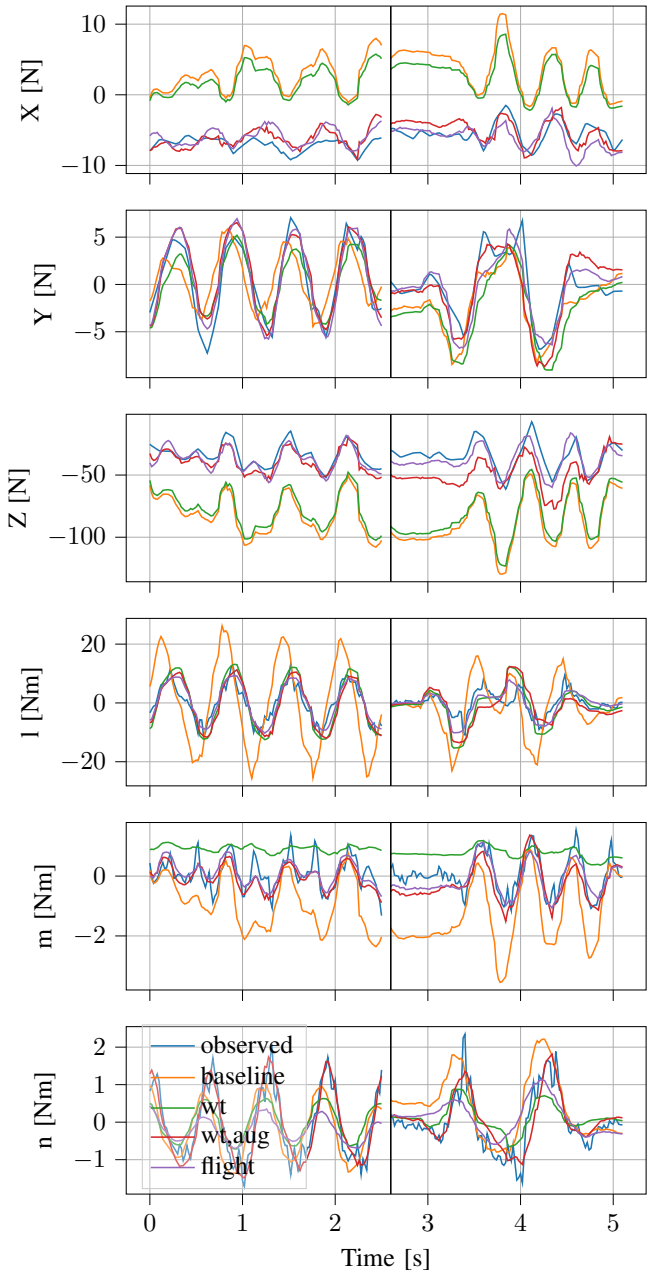

Fig. 6. Forces for aileron disturbances. The chirp disturbance was active during the first half and the step disturbance during the second half.

V. CONCLUSION

In this paper, we looked at the shortcomings of the existing model that we used for the dynamic model of a low-level nonlinear model predictive controller (NMPC). A calibration procedure that finds a static transformation for the wind tunnel data and a more careful consideration of the subset of data in which the aerodynamic coefficients are linear helped to improve the model compared to the baseline model [1]. Additional damping augmentation using SINDy further lifted the quality of the model which we demonstrated using flight

TABLE IV
THE R^2 SCORES FOR THE ENTIRE FLIGHT, INCLUDING THE MODELED AERODYNAMIC FORCES AND THE RESULTING ACCELERATIONS.

	X	Y	Z	l	m	n	$\dot{u}$	$\dot{v}$	$\dot{w}$	$\dot{p}$	$\dot{q}$	$\dot{r}$
baseline	-3	-0.27	-1.5	-3.1	-1.3	-0.63	-1.3	0.93	-0.19	-3.1	-1.3	-0.62
wt	-1.6	-0.5	-1	0.093	-0.096	0.21	-0.52	0.91	0.036	0.089	-0.096	0.036
wt,aug	0.68	0.12	0.63	-0.76	0.7	0.37	0.69	0.94	0.82	-0.77	0.7	0.26
flight	0.71	0.24	0.81	0.6	0.72	-0.0047	0.65	0.95	0.91	0.6	0.72	-0.26

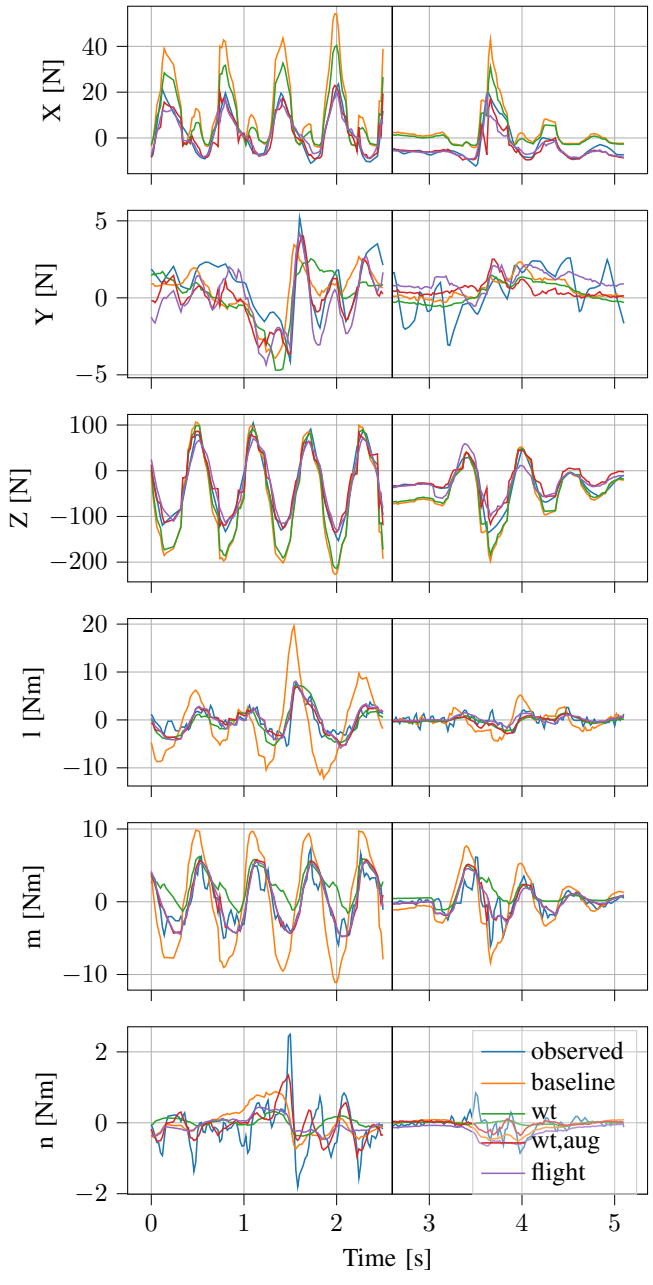

Fig. 7. Forces for elevator disturbances. The chirp disturbance was active during the first half and the step disturbance during the second half.

observations. We also used SINDy to identify a model that is entirely based on in-flight data collections, which does not require access to a wind tunnel and therefore helps to significantly reduce cost and effort. We discussed the implications of the additional complexity in light of the model mismatch for model-based control. However, a more rigorous design of the test campaign may improve the model quality, in particular larger variations to the throttle and open-loop training sequences for the control surfaces are needed.

ACKNOWLEDGMENT

We would like to thank Martin Sollie and Pål Kvaløy for their respective roles as operator and pilot in the experiments. Their support was essential in the data collections for this work. The discussions on general topics in systems identification with Erlend M. Coates are also appreciated. Finally, we would like to thank Petr Vrchota and Robert Kulhánek at VZLU for invaluable guidance in the experiment design and in performing the wind tunnel tests.

REFERENCES

[1] K. Gryte, R. Hann, M. Alam, J. Rohác, T. A. Johansen, and T. I. Fossen, "Aerodynamic modeling of the Skywalker X8 Fixed-Wing Unmanned Aerial Vehicle," *International Conference of Unmanned Aerial Systems*, 2018.

[2] K. Gryte, "Precision control of fixed-wing UAV and robust navigation in GNSS-denied environments," Ph.D. dissertation, Norwegian University of Science and Technology (NTNU), June 2020. [Online]. Available: https://hdl.handle.net/11250/2657113

[3] E. M. Coates, A. Wenz, K. Gryte, and T. A. Johansen, "Propulsion System Modeling for Small Fixed-Wing UAVs," in *2019 International Conference on Unmanned Aircraft Systems (ICUAS)*, 2019.

[4] D. Reinhardt, M. D. Pedersen, K. Gryte, and T. A. Johansen, "A symmetry calibration procedure to compensate for sensor-to-airframe misalignments in wind tunnel data," in *2022 Conference on Control Technologies and Applications (CCTA)*, submitted.

[5] K. Gryte, "High angle of attack landing of an unmanned aerial vehicle," Master's thesis, Department of Engineering Cybernetics, Norwegian University of Science and Technology, Trondheim, Norway, 2015.

[6] R. Mohammadi Farhadi, V. Kortunov, A. Molchanov, T. Solianyk *et al.*, "Estimation of the lateral aerodynamic coefficients for skywalker x8 flying wing from real flighttest data," 2018.

[7] Z. F. T. Gan, J. K. Feng, F. Khouli, M. S. ElSayed, and F. Nitzsche, "Development and optimization of flight dynamics, control laws and avionics system for a uav with a multi-scale optimized blended wing body configuration," *CASI Aero'19*, 2019.

[8] A. Winter, R. Hann, A. Wenz, K. Gryte, and T. A. Johansen, "Stability of a flying wing uav in icing conditions," in *8th European Conference for Aeronautics and Space Sciences (EUCASS), Madrid*, 2019.

[9] V. Klein, *Aircraft System Identification - Theory and Practice*. AIAA, 2006.

[10] R. V. Jategaonkar, *Flight Vehicle System Identification : A Time-domain Methodology*, 2nd ed. AIAA, 2015.

[11] G. Licitra, A. Bürger, P. Williams, R. Ruiterkamp, and M. Diehl, "Aerodynamic model identification of an autonomous aircraft for airborne wind energy," *Optimal Control Applications and Methods*, 2019.

[12] B. M. Simmons, H. G. McClelland, and C. A. Woolsey, "Nonlinear model identification methodology for small, fixed-wing, unmanned aircraft," *Journal of Aircraft*, vol. 56, no. 3, pp. 1056–1067, 2019. [Online]. Available: https://doi.org/10.2514/1.C035160

[13] J. J. Matt, S. G. Hagerott, B. C. Svoboda, H. Chao, and H. P. Flanagan, "Frequency domain system identification of a small flying-wing uas," in *AIAA SCITECH 2022 Forum*, 2022, p. 2407.

[14] M. B. Tischler and R. K. Remple, *Aircraft and rotorcraft system identification*. American Institute of Aeronautics and Astronautics Reston, VA, 2012.

[15] E. Kaiser, J. N. Kutz, and S. L. Brunton, "Sparse identification of nonlinear dynamics for model predictive control in the low-data limit," *Proceedings of the Royal Society A: Mathematical, Physical and Engineering Sciences*, vol. 474, no. 2219, p. 20180335, 2018. [Online]. Available: https://royalsocietypublishing.org/doi/abs/10.1098/rspa.2018.0335

[16] S. L. Brunton, J. L. Proctor, and J. N. Kutz, "Discovering governing equations from data by sparse identification of nonlinear dynamical systems," *Proceedings of the National Academy of Sciences*, vol. 113, no. 15, pp. 3932–3937, 2016. [Online]. Available: https://www.pnas.org/content/113/15/3932

[17] B. de Silva, K. Champion, M. Quade, J.-C. Loiseau, J. Kutz, and S. Brunton, "Pysindy: A python package for the sparse identification of nonlinear dynamical systems from data," *Journal of Open Source Software*, vol. 5, no. 49, p. 2104, 2020. [Online]. Available: https://doi.org/10.21105/joss.02104